

Analytical Study of (Ag–Graphene)/Blood Hybrid Nanofluid Influenced by (Platelets-Cylindrical)_{nanoparticles} and Joule Heating via VIM

Asla A. AL-Zahrani, Adnan,* Ishtiaque Mahmood, Khaleeq ur Rahman, Mutasem Z. Bani-Fwaz, and Elsayed Tag-Eldin



Cite This: *ACS Omega* 2023, 8, 19926–19938



Read Online

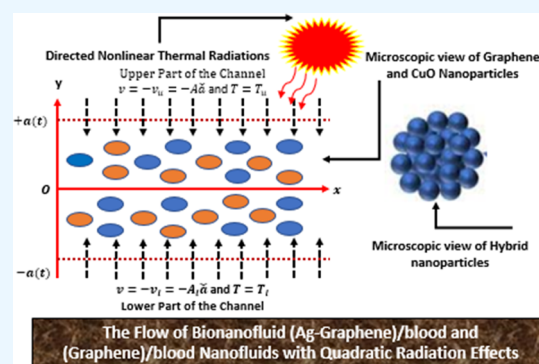
ACCESS |

Metrics & More

Article Recommendations

ABSTRACT: *Applications:* Flow-through permeable media have a wide range of applications in biomedical engineering, geophysical fluid dynamics, and recovery and refinement of underground reservoirs and large-scale chemical applications such as filters, catalysts, and adsorbents. Therefore, this study on a nanoliquid in a permeable channel is conducted under physical constraints. *Purpose and Methodology:* The key purpose of this research is to introduce a new biohybrid nanofluid model (BHNFM) with (Ag–G)_{hybridnanoparticles} with additional significant physical effects of quadratic radiation, resistive heating, and magnetic field. The flow configuration is set between the expanding/contracting channels, which has broad applications, especially in biomedical engineering. The modified BHNFM was achieved after the implementation of the bitransformative scheme, and then to obtain physical results of the model, the variational iteration method was applied.

Core Findings: Based on a thorough observation of the presented results, it is determined that the biohybrid nanofluid (BHNFM) is more effective than mono-nano BHNFs in controlling fluid movement. The desired fluid movement for practical purposes can be achieved by varying the wall contraction number ($\alpha_1 = -0.5, -1.0, -1.5, -2.0$) and with stronger magnetic effects ($M = 1.0, 9.0, 17.0, 25.0$). Furthermore, increasing the number of pores on the surface of the wall causes the BHNFM particles to move very slowly. The temperature of the BHNFM is affected by the quadratic radiation (R_q), heating source (Q_1), and temperature ratio number (θ), and this is a dependable approach to acquire a significant amount of heat. The findings of the current study can aid in a better understanding of parametric predictions in order to produce exceptional heat transfer in BHNFs and suitable parametric ranges to control fluid flow inside the working area. The model results would also be useful for individuals working in the fields of blood dynamics and biomedical engineering.



1. INTRODUCTION

Nanofluids have piqued the interest of researchers and scientists due to their promising properties in comparison to regular fluids. These fluids have exceptional heating/cooling properties, making them more useful for practical uses. As a result, researchers have concentrated on the synthesis of nanoparticles with varied properties and the production of nanofluids. In 2018, Mashayekhi et al.¹ described the use of bicomponent nanofluids in the formation of a bilayered wavy micro heat sink.^{2,3} The authors used Al₂O₃–Cu nanoparticles with water as the main solvent. They employed a CFD approach to simulate the model and discovered that a low Reynold number and a hot surface have a significant impact on the stationary thermal distribution. He et al.⁴ investigated the thermal conductivity of ZnO–Ag saturated in a hybrid base solvent with a contribution of 50–50%. They used artificial neural networks (ANNs) to estimate thermal conductivity. In 2020, Toghraie⁵ conducted an experimental analysis of a newly developed class known as

ternary nanofluids (TNFs). The ternary nanoparticles MWCNTs–titania–ZnO were used in the formation of the nanofluid. The experiment was carried out with mono-nano, bihybrid, and ternary nanofluids. The basic fluid is considered as a mixture of water and EG (80:20), and the ternary, mono-nano, and bihybrid nanofluids are made with nanoparticle concentrations ranging from 0.1 to 0.4%.

In 2020, Kristiawan et al.⁶ used TiO₂/w to improve the performance of a helical microfin tube. The authors investigated how to improve pressure drop by strengthening *Re* and reported

Received: March 21, 2023

Accepted: May 5, 2023

Published: May 19, 2023



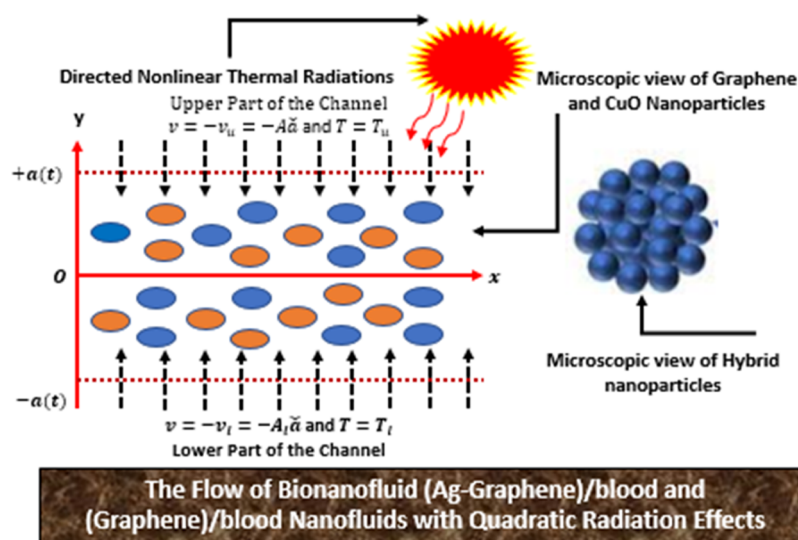


Figure 1. Bionanofluids (Ag-graphene)/blood and (graphene)/blood nanofluids.

on how to improve the performance of helical microfins utilizing nanofluids. Another significant analysis regarding heat transfer in TiO_2/w by considering squared minichannels containing microfin objects was carried out by Kristiawan et al.⁷ The authors recommended the use of nanofluids in microfins for practical applications due to their excellent heat transport. Recently, Kurnia et al.⁸ introduced a non-Newtonian nanoliquid model to assess its heat transmission ability in two separate heat exchangers of straight and helical types. It was found that helical-type heat exchangers had promising heat transmission properties when employing non-Newtonian fluids. Non-Newtonian fluids, like Newtonian nanofluids, have piqued the interest of researchers due to their challenging rheological properties. Significant research^{9,10} in this area has been conducted, examining the intriguing thermal behavior of the working fluid. In 2022, Muhammad et al.¹¹ and Zhang et al.¹² reported the uses of bihybrid nanofluids in solar energy plants as well as the influence of nonlinear quadratic radiations and Lorentz forces on frictional fluid flow. They favored the spectral approach for the mathematical treatment of the models and discussed the results comprehensively.

Hybrid nanofluids are extended versions of conventional mono-nanoliquids. As a result of the contribution of uniformly dispersed nanoparticles into the host fluid, the thermal conductivity of the resultant fluid is enhanced. These enhanced characteristics make the hybrid nanofluids more functional in comparison to nanoliquids. The most recent studies in the field of nano, hybrid, and ternary nanofluids have been reported by different researchers around the globe.^{13–16} Scientists have made efforts to explore the functioning of hybrid nanofluids under physically established conditions. In the presence of a transverse magnetic field, Ganesh et al.¹⁷ studied the steady laminar flow of a fluid between two permeable parallel plates. The fluid conducts electricity, is viscous, and is incompressible. In 2013, Ibrahim and Shankar¹⁸ discussed the heat transmission in boundary flow over a stretched permeable sheet with magnetic field effects and analyzed the influence of the considered physical constraints.

In 2014, Srinivas et al.¹⁹ examined the nanofluid hydro-magnetic flow in a two-dimensional permeable region. The effects of numerous parameters were also analyzed, and the results show that the concentration of nanoparticles is directly

correlated to the Brownian factor. In 2014, Hafeez et al.²⁰ investigated the two-dimensional (2D) nontransient laminar flow in a permeable medium. The results for the least and largest Reynolds number ranges were discussed in depth. In 2015, Fakour et al.²¹ studied the heat transfer mechanism and laminar fluid flow between two parallel porous plates. The influence of dimensionless parameters on the dimensionless velocity and temperature profiles has also been studied.

In 2016, Mollamahdi et al.²² investigated the heat transfer and flow field between permeable channels with hybrid nanofluid^{23–25} under the influence of a magnetic field and chemical reaction. They found that with an increase in the Hartman parameter, the temperature profile declines, and the concentration of the fluid increases. In 2016, Vijayalakshmi et al.²⁶ studied the heat transmission mechanism of the contracting or stretching parallel porous channels in response to thermal radiation. In 2017, Fakour et al.²⁷ investigated the conduction of heat in the laminar flow of fluid between permeable walls in the presence of a magnetic field. Effects of nondimensional parameters were studied, and the results showed that an increase in the Hartman and Reynolds numbers causes a reduction in the velocity of the fluid, while an increase in values of the Eckert and Prandtl numbers increases the temperature. In 2019, Mehta et al.²⁸ analyzed the heat and radiation effects on the unsteady MHD flow in a permeable medium. The graphical analysis shows that the temperature increases with an increase in volume fraction.

The study reported by Chandrasekar et al.²⁹ revealed that particle movement can be controlled under the effects of a transverse magnetic field with the injection process at the bottom and suction at the top of the channel. Studies on a variety of newly developed nanofluids composed of different basic fluids have been reported.^{30–33} In 2019, Waini et al.³⁴ achieved steady fluid flow with heat transformation through a porous shrinking/stretching surface. The results demonstrated that an increase in the volume fraction tends to decrease the skin friction values but enhances the values of the Nusselt number for both nanofluids and hybrid nanofluids. Khan et al.³⁵ investigated 2D steady laminar flow in permeable media and analyzed the porosity effects on the model dynamics.

In 2022, Indumathi et al.³⁶ examined a hybrid nanofluid with a permeable surface under the suction and injection process. The

results of the physical model showed that increasing the number of nanoparticles in the basic fluid will result in a decrease in the velocity of hybrid nanofluids.^{37–40} In 2022, Mburu et al.⁴¹ investigated the unsteady, two-dimensional, viscous, and incompressible flow of the boundary layer of an electrically conducting nanofluid through porous plates. Bivariate spectral quasilinearization (BSQL) was used for the model study. In 2023, Shaheen et al.⁴² discussed nanofluid and MHD hybrid nanofluid^{43–46} flow between parallel plates under the effects of thermal radiation and a magnetic field. Both plates are porous for the injection and suction process, which significantly contributed to the heat and momentum transmission of the fluid.

The above literature reveals that there are many studies reported on the use of simple and hybrid nanoparticles by considering traditional fluids and restricting physical constraints. However, the interaction of Ag and graphene nanoparticles with blood is significant in the field of biomedical engineering, which has not been reported so far. Thus, a biohybrid nanofluid model using bicomponents (platelets-cylindrical)_{nanoparticles} in a channel with permeable effects has not been investigated to date. This important research gap motivated the authors to pursue this potential research opening. Furthermore, magnetic field, Joule heating, and heating source effects were incorporated to enhance the novelty of the study and to examine the behavior of the bionanofluid. First, the biohybrid nanofluid model, developed by exercising the similarity transformation rules, enhanced the properties of the nanoliquid and shape factor of (Ag–graphene) nanoparticles. Then, the model was resolved using an analytical scheme following the variational iteration method (VIM). In the end, the impact of the ingrained physical constraints on the model dynamics was studied and discussed comprehensively.

2. MODEL DEVELOPMENT

2.1. Model Statement and Geometry. The (Ag + Graphene) hybrid nanofluid with blood as the base fluid was

Table 1. Particular Values of Thermophysical Factors for the Formation of the Biohybrid Nanofluid Model

| working fluid/nanoparticles | characteristics | | |
|-----------------------------|-----------------------------|-------------|------------|
| | ρ (kg/m ³) | C_p (J/K) | k (W/mK) |
| blood | 1063 | 3594 | 0.492 |
| Ag (platelet) | 10,500 | 235 | 429 |
| graphene (cylindrical) | 2200 | 790 | 5000 |

made to flow between two permeable walls at $y = -a(t)$ and $y = a(t)$, respectively, in the presence of a magnetic field. The model is developed in a way that u and v are in the directions of the x -axis and y -axis, respectively. The entire model under consideration in this study is represented in Figure 1.

2.1.1. Assumptions. The following are the essential limitations of the study to acquire the model results:

- The flow of the biohybrid nanoliquid in the channel is laminar, viscous, and incompressible.
- The bicomponent particles (Ag–graphene) dissolved uniformly in blood, and no chemical reaction exists between them.
- The fluid consistently moves through permeable walls, and the channel plates are positioned at $a(t)$ and $-a(t)$.
- The walls are capable of expanding/contracting uniformly.

The governing set of equations for the above-described flow configuration is as below

$$\frac{\partial \tilde{u}}{\partial x} + \frac{\partial \tilde{v}}{\partial y} = 0 \quad (1)$$

$$\begin{aligned} \rho_{\text{hbionanof}} \left(\frac{\partial \tilde{u}}{\partial t} + \tilde{u} \frac{\partial \tilde{u}}{\partial \tilde{x}} + \tilde{v} \frac{\partial \tilde{u}}{\partial \tilde{y}} \right) \\ = -\frac{\partial \tilde{P}}{\partial \tilde{x}} + \mu_{\text{hbionanof}} \left[\frac{\partial^2 \tilde{u}}{\partial \tilde{x}^2} + \frac{\partial^2 \tilde{u}}{\partial \tilde{y}^2} \right] - \sigma_{\text{hbionanof}} B_0^2 \tilde{u} \end{aligned} \quad (2)$$

$$\begin{aligned} \rho_{\text{hbionanof}} \left(\frac{\partial \tilde{v}}{\partial t} + \tilde{u} \frac{\partial \tilde{v}}{\partial \tilde{x}} + \tilde{v} \frac{\partial \tilde{v}}{\partial \tilde{y}} \right) \\ = -\frac{\partial \tilde{P}}{\partial \tilde{y}} + \mu_{\text{hbionanof}} \left[\frac{\partial^2 \tilde{v}}{\partial \tilde{x}^2} + \frac{\partial^2 \tilde{v}}{\partial \tilde{y}^2} \right] - \sigma_{\text{hbionanof}} B_0^2 \tilde{v} \end{aligned} \quad (3)$$

$$\begin{aligned} (\rho C_p)_{\text{hbionanof}} \left(\frac{\partial \tilde{T}}{\partial t} + \tilde{u} \frac{\partial \tilde{T}}{\partial \tilde{x}} + \tilde{v} \frac{\partial \tilde{T}}{\partial \tilde{y}} \right) \\ = k_{\text{hbionanof}} \left[\frac{\partial^2 \tilde{T}}{\partial \tilde{x}^2} + \frac{\partial^2 \tilde{T}}{\partial \tilde{y}^2} \right] + Q_0 (\tilde{T} - \tilde{T}_0) \\ - \sigma_{\text{hbionanof}} B_0^2 (\tilde{u}^2 + \tilde{v}^2) \end{aligned} \quad (4)$$

In the above coupled governing system, conservation of mass is given by eq 1, the two components of the momentum equation are described in eqs 2 and 3, and the conservation of energy is given in eq 4. More details on the conservation of energy have been provided by different researchers.^{47,48}

The flow configuration depicted in Figure 1 is restricted to the subsequent boundary rules

$$\left\{ \begin{array}{l} \tilde{u} = 0, T \\ = T_l, \tilde{v} \\ = -v_l \\ = -hA_l \text{ at lower end } (\tilde{y} \\ = -h(t)) \\ \tilde{u} = 0, T \\ = T_u, \tilde{v} \\ = -v_u \\ = -hA_u \text{ at upper end } (\tilde{y} \\ = h(t)) \end{array} \right. \quad (5)$$

Now, for further simplification, the vorticity for the model is given as follows

$$\chi = \frac{\partial \tilde{v}}{\partial \tilde{x}} - \frac{\partial \tilde{u}}{\partial \tilde{y}} \quad (6)$$

To remove the gradient of pressure from eqs 2 and 3, we apply cross-differentiation and obtain the subsequent formula

$$\begin{aligned} \rho_{\text{hbionanof}} \left(\frac{\partial \tilde{\chi}}{\partial t} + \tilde{u} \frac{\partial \tilde{\chi}}{\partial \tilde{x}} + \tilde{v} \frac{\partial \tilde{\chi}}{\partial \tilde{y}} \right) \\ = \mu_{\text{hbionanof}} \left[\frac{\partial^2 \tilde{\chi}}{\partial \tilde{x}^2} + \frac{\partial^2 \tilde{\chi}}{\partial \tilde{y}^2} \right] - \sigma_{\text{hbionanof}} B_0^2 \frac{\partial \tilde{\chi}}{\partial \tilde{y}} \end{aligned} \quad (7)$$

The required results are as follows

$$\begin{aligned} & \rho_{\text{hbionanof}}(\tilde{u}_{yt} + \tilde{u}_{yx} + \tilde{v}_{yy}) \\ &= \mu_{\text{hbionanof}}\tilde{u}_{yyy} - \sigma_{\text{hbionanof}}B_0^2\tilde{u}_{yy} \end{aligned} \quad (8)$$

Now, we introduce the proximate transfiguration parameters to reduce the above expressions into a more compressed form

$$y = \eta h \quad (9)$$

$$\begin{aligned} \tilde{u} &= \frac{v_f \tilde{x} \tilde{f}_\eta}{h^2}, \tilde{v} = -\frac{v_f \tilde{f}(\eta, t)}{h}, \tilde{\psi} = -\frac{v_f \tilde{x} \tilde{f}(\eta, t)}{h}, \theta(\eta) \\ &= \frac{\tilde{T} - \tilde{T}_u}{\tilde{T}_i - \tilde{T}_u} \end{aligned} \quad (10)$$

After using the transformations from eq 10, the reduced BCs are listed as follows

$$\begin{cases} \tilde{f}_\eta = 0, \tilde{f} = Re, Re = \frac{hh \cdot A_u}{v_f} \text{ at } \eta = -1 \\ \tilde{f}_\eta = 0, \tilde{f} = Re, Re = \frac{hh \cdot A_u}{v_f} \text{ at } \eta = 1 \end{cases} \quad (11)$$

It is well-known that positive/negative values of the Reynolds number (Re) are correlated to injection/suction. Now, it is quite useful to establish a second set of parameters to build our model in a manageable form.

$$u = \frac{\tilde{u}}{h}, v = \frac{\tilde{v}}{h}, x = \frac{\tilde{x}}{h}, f = \frac{\tilde{f}}{Re} \quad (12)$$

2.2. Biohybrid Nanofluid Components and their Characteristics. For (Ag–graphene)/blood and (graphene)/blood nanofluids, the subsequent expressions are used. These formulas are valid for platelets and cylindrical-shaped nanoparticles.

2.2.1. Bionanofluid Density (BD).

$$\frac{\rho_{\text{hbionanof}}}{\rho_{\text{blood}}} = (1 - \phi_{\text{Ag}} - \phi_{\text{G}}) + \frac{\phi_{\text{Ag}}\rho_{\text{Ag}}}{\rho_{\text{blood}}} + \frac{\phi_{\text{G}}\rho_{\text{G}}}{\rho_{\text{blood}}} \quad (13)$$

2.2.2. Bionanofluid Heat Capacitance (BHC).

$$\begin{aligned} \frac{(\rho C_p)_{\text{hbionanof}}}{(\rho C_p)_{\text{blood}}} &= (1 - \phi_{\text{Ag}} - \phi_{\text{G}}) + \frac{\phi_{\text{Ag}}(\rho C_p)_{\text{Ag}}}{(\rho C_p)_{\text{blood}}} \\ &+ \frac{\phi_{\text{G}}(\rho C_p)_{\text{G}}}{(\rho C_p)_{\text{blood}}} \end{aligned} \quad (14)$$

2.2.3. Bionanofluid Dynamic Viscosity (BDV). The viscosity models for (PP+CP)/(platelet and cylindrical) nanoparticles are defined as follows

$$\frac{(\mu_{\text{bionanof}})_{\text{Ag}}}{\mu_{\text{blood}}} = (1 + 37.1\phi + 612.6\phi^2)$$

valid for PNP (platelet nanoparticles) (15)

$$\frac{(\mu_{\text{bionanof}})_{\text{G}}}{\mu_{\text{blood}}} = (1 + 13.5\phi + 904.5\phi^2)$$

valid for CNP (cylindrical nanoparticles) (16)

$$\mu_{\text{hbionanof}} = \frac{(\mu_{\text{bionanof}})_{\text{Ag}}\phi_{\text{Ag}} + (\mu_{\text{bionanof}})_{\text{G}}\phi_{\text{G}}}{\phi_{\text{Ag}} + \phi_{\text{G}}}$$

resultant HBNF (hybrid bionanofluid) (17)

2.2.4. Bionanofluid Thermal Conductivity (BTC). The thermal conductivity of bionanofluids is estimated using the following relations

$$\frac{(k_{\text{hbionanof}})_{\text{Ag}}}{k_{\text{blood}}} = \frac{k_{\text{Ag}} + 4.7k_{\text{blood}} + 4.7\phi_{\text{Ag}}(k_{\text{Ag}} - k_{\text{blood}})}{k_{\text{Ag}} + 4.7k_{\text{blood}} - \phi_{\text{Ag}}(k_{\text{Ag}} - k_{\text{blood}})}$$

for PNP (platelet nanoparticles) (18)

$$\frac{(k_{\text{hbionanof}})_{\text{G}}}{k_{\text{blood}}} = \frac{k_{\text{G}} + 3.9k_{\text{blood}} + 3.9\phi_{\text{G}}(k_{\text{G}} - k_{\text{blood}})}{k_{\text{G}} + 3.9k_{\text{blood}} - \phi_{\text{G}}(k_{\text{G}} - k_{\text{blood}})}$$

for CNP (cylindrical nanoparticles) (19)

$$k_{\text{hbionanof}} = \frac{(k_{\text{bionf}})_{\text{Ag}} + (k_{\text{bionf}})_{\text{G}}}{\phi_{\text{Ag}} + \phi_{\text{G}}}$$

(hybrid bionanofluid) (20)

It is significant to combine the values of these bionanofluid characteristics (BHNF) because they greatly contribute to the dynamics of the bionanofluid. For this, Table 1 indicates the particular values of these factors.

2.3. (Ag–G)/Blood Biohybrid Nanofluid Model. We obtained the following equation by completing the mathematical procedure with transformative factors along with thermophysical characteristics of blood as the base fluid and (PP+CP) nanoparticles.

$$\begin{aligned} F''' + \frac{\rho_{\text{hbionanof}}/\rho_{\text{blood}}}{\mu_{\text{hbionanof}}/\mu_{\text{blood}}}((\eta F''' + 3F'')\alpha_1 \\ - R_1(F'F'' - FF''')) - \frac{1}{\mu_{\text{hbionanof}}/\mu_{\text{blood}}}R_1MF'' \\ = 0 \end{aligned} \quad (21)$$

$$F(\eta_1) = A_1, F'(\eta_1) = 0, F(\eta_u) = 1, F'(\eta_u) = 0 \quad (22)$$

In eq 14, η_1 and η_u indicate the bottom and top wall conditions, respectively. The converted energy equation is obtained by using transformations

$$\begin{aligned} \frac{k_{\text{hbionanof}}}{k_{\text{blood}}}\beta'' + P_r \frac{(\rho C_p)_{\text{hbionanof}}}{(\rho C_p)_{\text{blood}}}(\alpha_1\eta + R_1F)\beta' \\ - R_d((1 + (\theta_r - 1)\beta)^3\beta'' + 3(1 + (\theta_r - 1)\beta)^2(\beta')^2 \\ (\theta_r - 1)) + Q_r\beta + P_rM(F')^2 \\ = 0 \end{aligned} \quad (23)$$

$$\beta(-1) = 1, \beta(1) = 0 \quad (24)$$

where $Q = \frac{Q_0 a^2}{v_f(\rho C_p)_f}$ and $M = \frac{\sigma_r B_0^2 a^2}{\mu_f}$ are the heat source and magnetic variable terms, respectively.

2.4. Shear Drag and the Nusselt Modeling. The study of the drag force and local thermal gradient is very important in the analysis of bionanofluids. For the current model, these expressions are defined in the subsequent equations

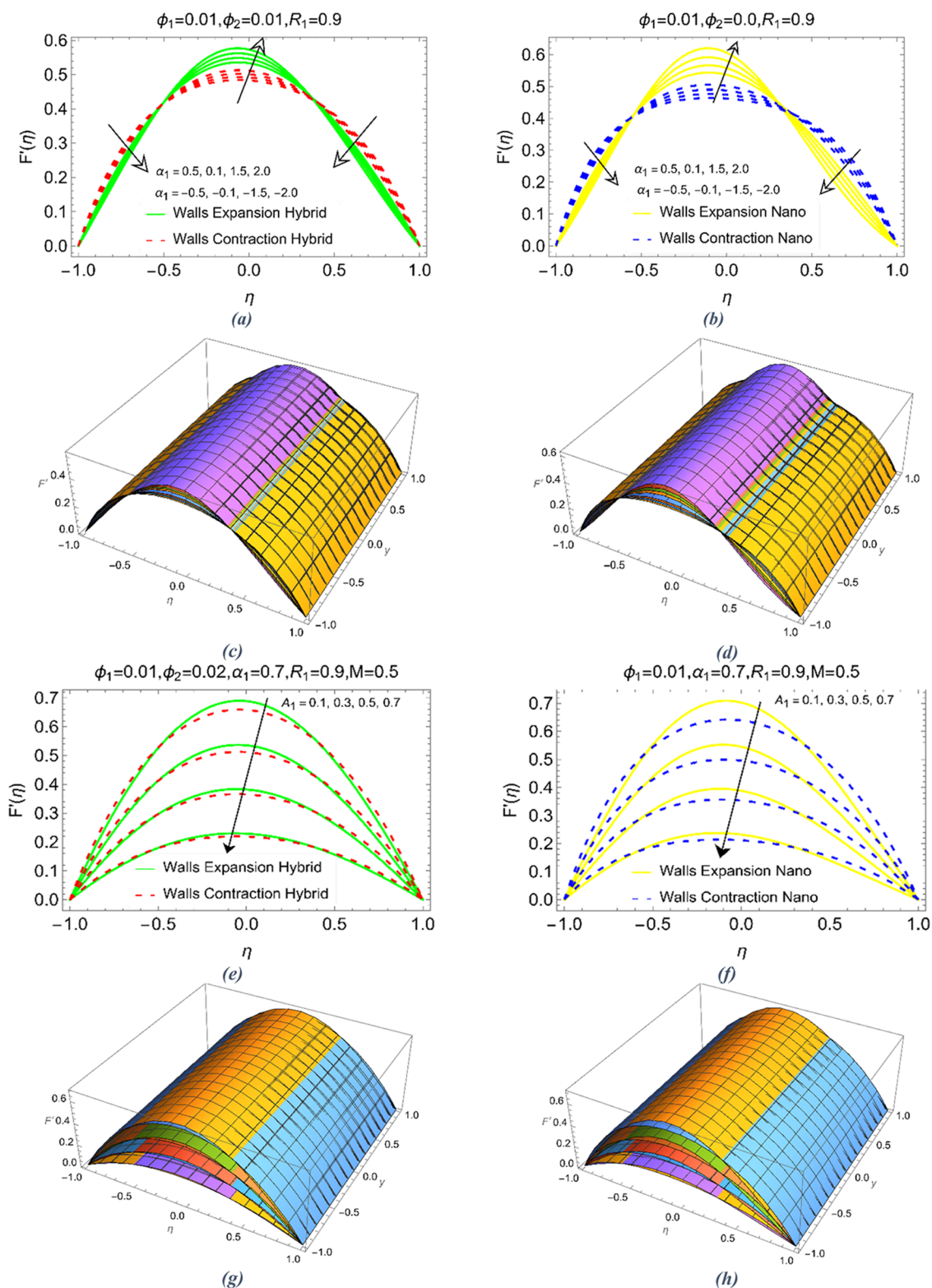


Figure 2. Velocity $F'(\eta)$ of α_1 for (a) Hybrid and (b) Nano; 3D views of (c) Hybrid and (d) Nano; A_1 of (e) Hybrid and (f) Nano; 3D views for A_1 of (g) Hybrid and (h) Nano.

$$C_F = \frac{\tau a(t)}{\rho_{\text{hbionanof}} v_1^2}, \quad \tau_w = \mu_{\text{hbionanof}} \left[\frac{\partial \tilde{u}}{\partial y} \right] \text{ when } y = \mp a \quad (25)$$

$$N_u = \frac{a}{k_f(T_1 - T_u)} \left[\frac{k_{\text{hbionanof}} \partial T}{\partial y} + q_{\text{rd}} \right] \text{ when } y = \mp a \quad (26)$$

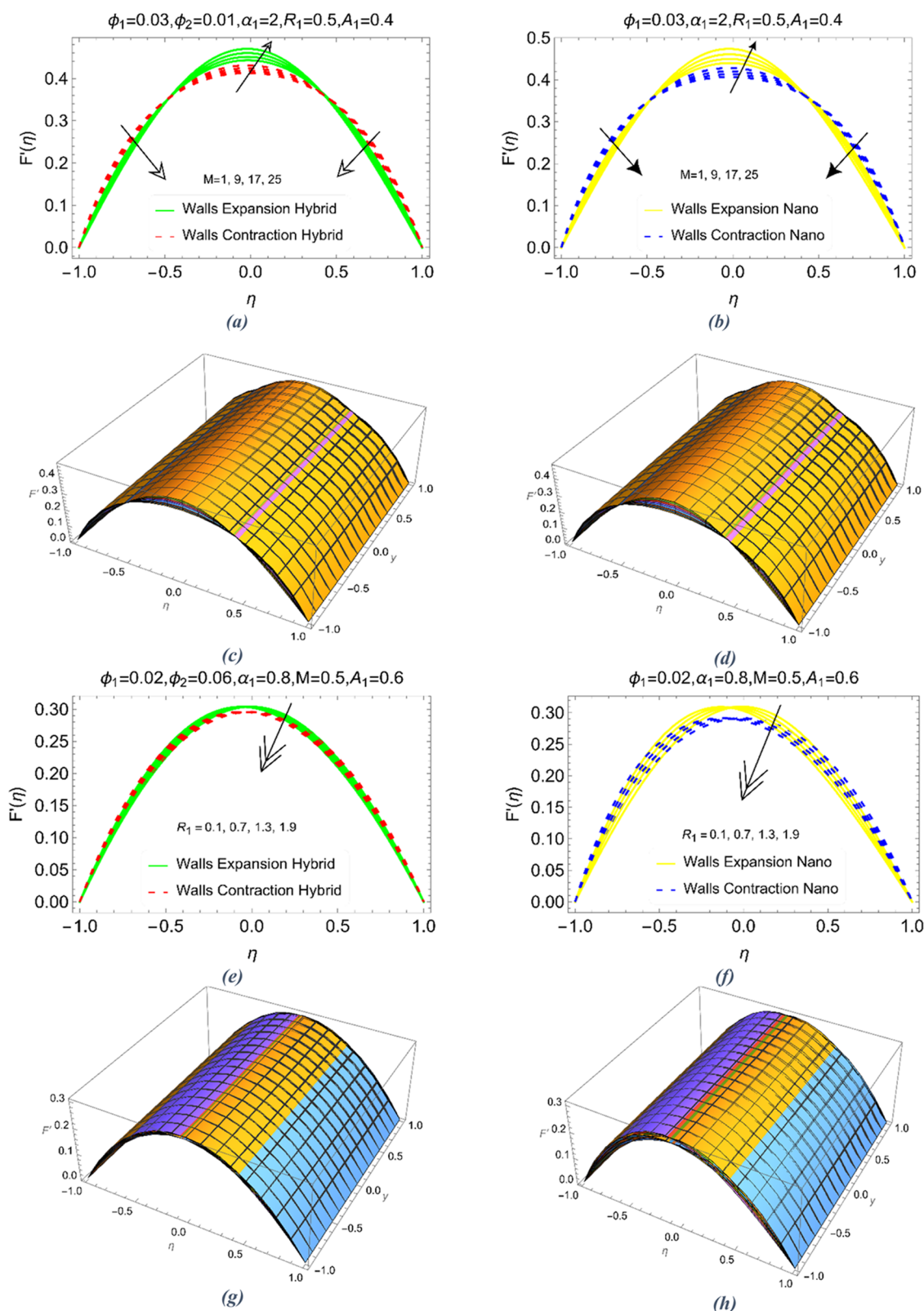


Figure 3. Velocity $F'(\eta)$ of the biohybrid nanofluid against M for (a) Hybrid (b) Nano; 3D views of (c) Hybrid and (d) Nano; R_1 of (e) Hybrid and (f) Nano; 3D views of R_1 of (g) Hybrid and (h) Nano.

Using the biohybrid nanofluid expressions along with the transformative factors, the following dimensionless formulae were achieved

$$R_1^2 C_{Fl} = \frac{\left[\frac{(\mu_{\text{bionanof}})_{Ag} \phi_{Ag} + (\mu_{\text{bionanof}})_G \phi_G}{\phi_{Ag} + \phi_G} \right] F''(-1)}{\left[(1 - \phi_{Ag} - \phi_G) + \frac{\phi_{Ag} \rho_{Ag}}{\rho_{\text{blood}}} + \frac{\phi_G \rho_G}{\rho_{\text{blood}}} \right]} \quad (27)$$

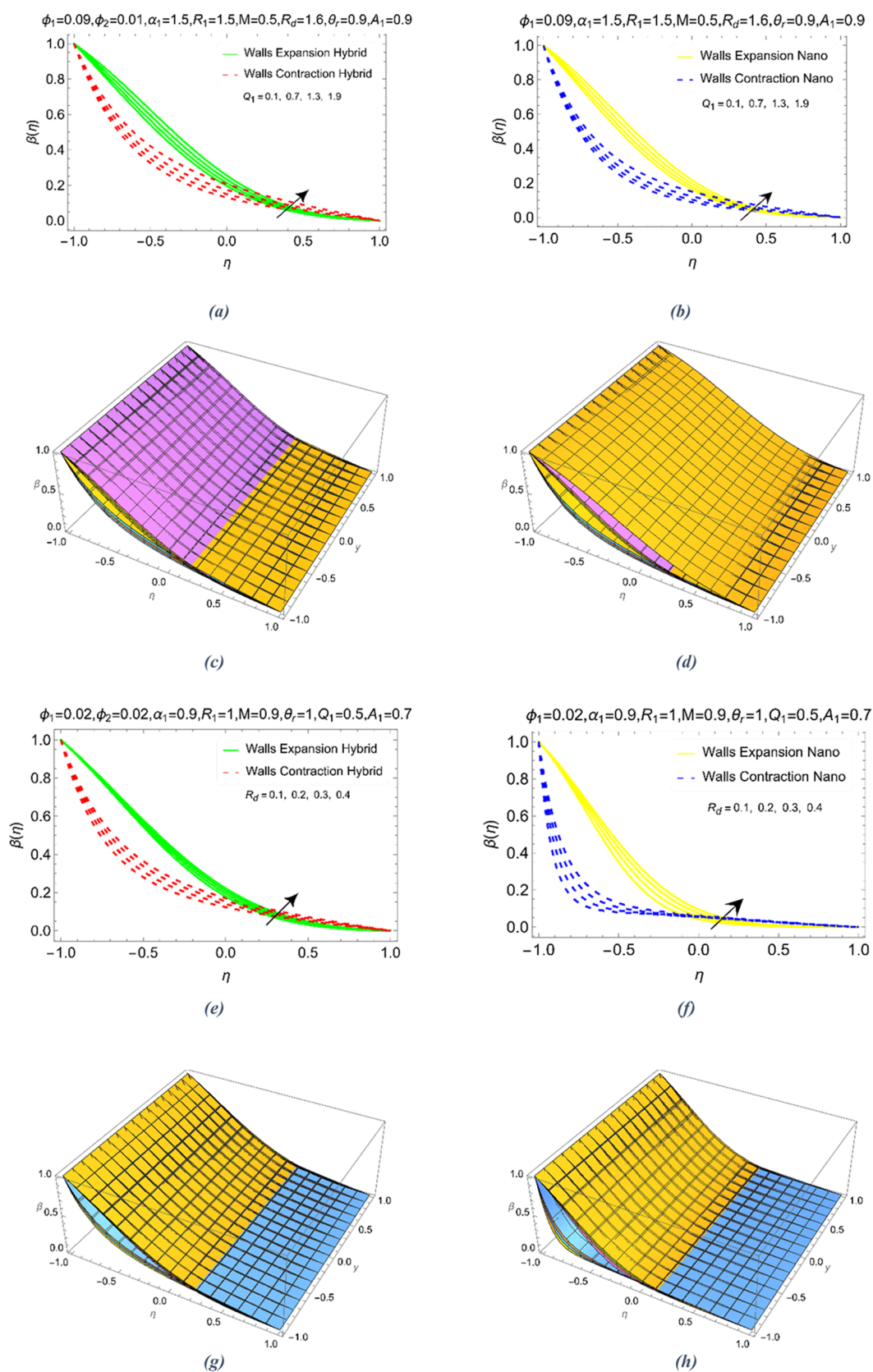


Figure 4. continued

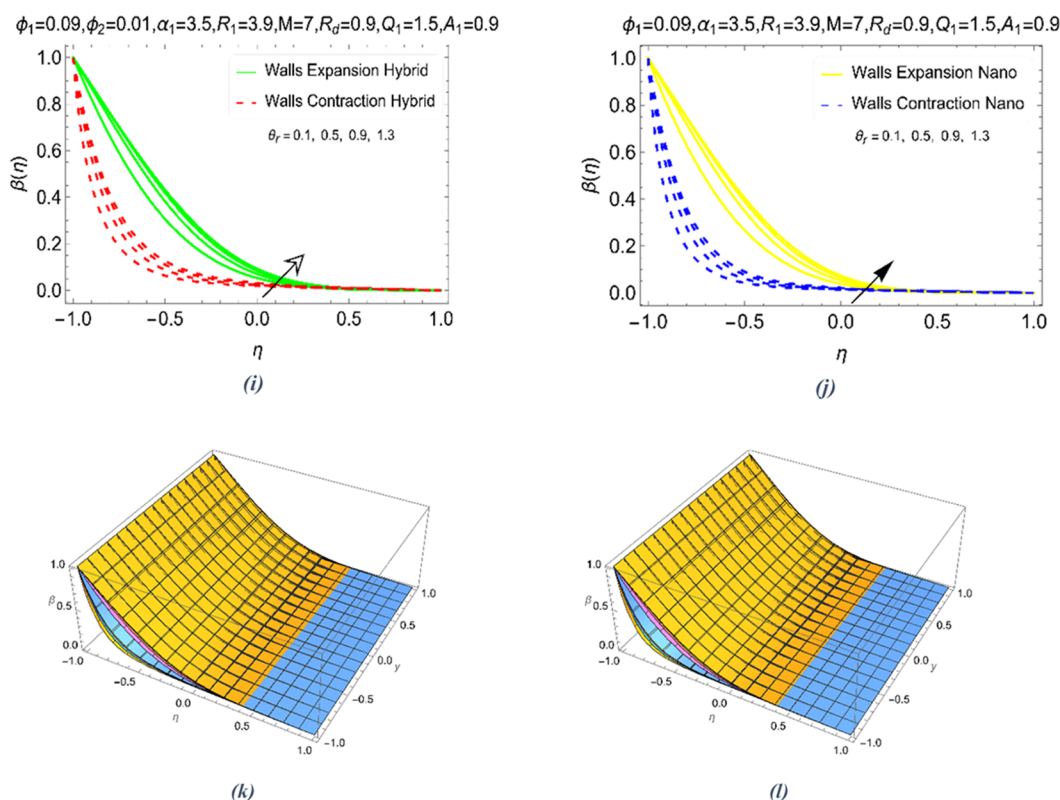


Figure 4. Thermal view $\beta(\eta)$ of biohybrid nanofluid against Q_1 for (a) Hybrid (b) Nano; 3D views of (c) Hybrid and (d) Nano; R_d of (e) Hybrid and (f) Nano; 3D views of R_d of (g) Hybrid and (h) Nano; θ_r of (i) Hybrid and (j) Nano; and 3D view of θ_r of (k) Hybrid and (l) Nano.

$$R_u^2 C_{Fu} = \frac{\left[\frac{(\mu_{\text{bionanof}})_{Ag} \phi_{Ag} + (\mu_{\text{bionanof}})_G \phi_G}{\phi_{Ag} + \phi_G} \right]}{\left[(1 - \phi_{Ag} - \phi_G) + \frac{\phi_{Ag} \rho_{Ag}}{\rho_{\text{blood}}} + \frac{\phi_G \rho_G}{\rho_{\text{blood}}} \right]} F''(1) \tag{28}$$

$$N_{ul} = \left| \beta'(-1) \left(\frac{(k_{\text{bionanof}})_{Ag} + (k_{\text{bionanof}})_G}{\phi_{Ag} + \phi_G} \right) + R_d (1 - (1 - \theta_r) \beta(-1))^3 \right| \tag{29}$$

$$N_{up} = \left| \beta'(1) \left(\frac{(k_{\text{bionanof}})_{Ag} + (k_{\text{bionof}})_G}{\phi_{Ag} + \phi_G} \right) + R_d (1 - (1 - \theta_r) \beta(1))^3 \right| \tag{30}$$

3. MATHEMATICAL INVESTIGATION VIA VIM

The considered biohybrid nanofluid model (Ag–G)/blood in the presence of PNP and CNP exhibits strong nonlinearities. Because of this, it is difficult for researchers to obtain exact solutions. Therefore, analytical techniques are the most suitable mathematical tools to compute the solution. Thus, the current biohybrid nanofluid model (BHNFM) is analyzed via the variational iteration method (VIM). Initially, the trial solution of the model is determined; then, successive approximations of the solution are performed via the recursive relation of velocity and

energy model equations. The detailed computational steps of the technique are presented below.

3.1. Arrangement of the Model Equations. The first step in the method implementation is the arrangement of the model equations in the appropriate form. Thus, the model can be arranged in the following form: the highest-order linear operator ($\check{\mathcal{L}}_1, \check{\mathcal{L}}_2$), linear terms ($\check{\mathcal{R}}_1, \check{\mathcal{R}}_2$), nonlinear factors ($\check{\mathcal{N}}_1, \check{\mathcal{N}}_2$), and the remaining nonhomogeneous ($\check{q}_1^*, \check{q}_2^*$) part of the model.

$$\check{\mathcal{L}}_1 F + \check{\mathcal{R}}_1 F + \check{\mathcal{N}}_1 F + \check{q}_1^*(\eta) = 0 \tag{31}$$

$$\check{\mathcal{L}}_2 \beta + \check{\mathcal{R}}_2 \beta + \check{\mathcal{N}}_2 \beta + \check{q}_2^*(\eta) = 0 \tag{32}$$

3.2. Appropriate Lagrange Multipliers. There will be two Lagrange multipliers for the current biohybrid nanofluid model because the model contains two equations. These multipliers are defined by the subsequent expressions

$$\check{\lambda}_F = \frac{(-1)^{n^*} (\eta - s)^{n^*-1}}{(n^* - 1)!} \tag{33}$$

$$\check{\lambda}_\beta = \frac{(-1)^{n^*} (\eta - s)^{n^*-1}}{(n^* - 1)!} \tag{34}$$

3.3. Initial Guess of the Model. The initial guesses of the model can be constructed using the initial conditions, i.e., conditions imposed at $\eta = 0$. In view of ICs of the model, these guesses are expressed as follows

$$F_0 = \sum_{i=0}^j \frac{\eta^i F(0)}{i!} \text{ and } \beta_0 = \sum_{i=0}^j \frac{\eta^i \beta(0)}{i!} \tag{35}$$

Table 2. Computations of Drag Forces for the Biohybrid Nanofluid at the Bottom and Top Ends of the Channel

| parameter changes | | | | | shear drag of BHNf at the boundaries versus the physical parameters | | | |
|-------------------|----------|-------|-----|-------|---|------------------------|----------------------|------------------------|
| ϕ_{Ag} | ϕ_G | R_1 | M | A_1 | $F''(-1)$ | | $ F''(1) $ | |
| | 0.03 | 3.0 | 0.5 | 0.6 | expanding boundaries | contracting boundaries | expanding boundaries | contracting boundaries |
| 0.04 | | | | | 1.1249 | 1.1582 | 0.7959 | 0.8287 |
| 0.08 | | | | | 1.0585 | 1.0801 | 0.8444 | 0.8659 |
| 0.12 | | | | | 1.0294 | 1.0457 | 0.8681 | 0.8843 |
| 0.16 | | | | | 1.0131 | 1.0263 | 0.8822 | 0.8953 |
| 0.04 | 0.01 | | | | 1.1572 | 1.1957 | 0.7793 | 0.8169 |
| | 0.03 | | | | 1.1249 | 1.1582 | 0.7959 | 0.8287 |
| | 0.05 | | | | 1.1058 | 1.1361 | 0.8062 | 0.8362 |
| | 0.07 | | | | 1.0933 | 1.1215 | 0.8133 | 0.8413 |
| | 0.03 | 2.0 | | | 1.0580 | 1.0918 | 0.8353 | 0.8688 |
| | | 4.0 | | | 1.1933 | 1.2262 | 0.7611 | 0.7931 |
| | | 6.0 | | | 1.3339 | 1.3660 | 0.7035 | 0.7338 |
| | | 8.0 | | | 1.4784 | 1.5096 | 0.6592 | 0.6875 |
| | | 3.0 | 0.1 | | 1.1147 | 1.1481 | 0.7814 | 0.8145 |
| | | | 0.3 | | 1.1198 | 1.1532 | 0.7887 | 0.8216 |
| | | | 0.5 | | 1.1249 | 1.1582 | 0.7959 | 0.8287 |
| | | | 0.7 | | 1.1299 | 1.1633 | 0.8030 | 0.8358 |
| | | | 0.5 | 0.2 | 2.1372 | 2.2031 | 1.6583 | 1.7231 |
| | | | | 0.4 | 1.6441 | 1.6939 | 1.2187 | 1.2677 |
| | | | | 0.6 | 1.1249 | 1.1582 | 0.7959 | 0.8287 |
| | | | | 0.8 | 0.5775 | 0.5943 | 0.3896 | 0.4062 |

Here, F_0 and β_0 are the guesses associated with the model equations.

3.4. Recursive Formula for the Final Model Solution.

The final solution of the model can then be achieved by means of the following recursive relations. The international scheme gives more accurate results by running the code at a higher number of iterations. These relations are well-defined as given below

$$F_{n+1} = F_0 + \int_{\eta}^0 \tilde{\lambda}_F(-\tilde{\mathcal{R}}_1 F(s) - \tilde{\mathcal{N}}_1 F(s) - \tilde{q}_1^*(s)) ds, n \geq 0 \quad (36)$$

$$\beta_{n+1} = \beta_0 + \int_{\eta}^0 \tilde{\lambda}_\beta(-\tilde{\mathcal{R}}_2 \beta(s) - \tilde{\mathcal{N}}_2 \beta(s) - \tilde{q}_2^*(s)) ds, n \geq 0 \quad (37)$$

4. RESULTS

The physical parameters that appear in the biohybrid nanofluid model (BHNFM) greatly affect the dynamics of the functional fluid in the geometry of interest. Therefore, this section is arranged to provide a deep analysis of the model dynamics under various parametric values.

5. DISCUSSION

This section provides a comprehensive discussion of the results furnished in the previous section under a variety of physical parameters.

Figure 2 displays a comparative piqued velocity distribution for bicomponent and monocomponent nanofluids against increasing parametric values. Figure 2a,b demonstrates the fluid movement in a permeable channel under the physical effects of α_1 . The two flow situations, i.e., expansion and contraction of the walls, are considered. From the demonstrated results, it is found that the fluid particles attain the maximum velocity at the center of the channel. However, it is rapid for elongated walls. Physically, the expansion of the walls provides

more working domain, and as a consequence, the particle movement is enhanced. The fluid behavior almost changes close to η values of -0.5 and 0.5 for hybrid and simple nanofluids, respectively. The physical cause for this phenomenon is the adverse pressure in the surroundings of the walls, which opposes the fluid motion. In the case of nanofluids, the velocity for both elongation and contraction is more rapid than that of hybrid nanofluids because a hybrid nanofluid is a denser medium than a simple nanofluid due to the binanoparticle density. Physically, increasing the density provides more frictional force inside the fluid layers. Thus, due to dominant frictional effects, the velocity of the bihybrid nanofluid increases slowly. Further, the velocity decreases near the walls as per the implication of boundary conditions. The three-dimensional (3D) pictorial view of Figure 2a,b is displayed in Figure 2c,d.

The significant influence of the permeability number A_1 on $F'(\eta)$ is demonstrated in Figure 2e,f for couple fluids. This parameter appeared due to the pores at the surface, which is physically described by the permeability number. The permeability condition on the channel walls results in a significant decrease in fluid movement. It is clear that on increasing the value of A_1 , the fluids move slowly, and the motion is limited. Physically, due to a high number of surface pores, the particles drag toward the free space. As a consequence, the velocity in the working region decreases. Further, the motion can be controlled by contracting the walls and strengthening the absorbent effects. Further, Figure 2g,h displays the 3D trends of Figure 2e,f.

The Hartmann number, which is a quotient of the electromagnetic force to the viscous force, is an important dimensionless number. This parameter appears in the models where the fluid flows under a directed magnetic field. Thus, the effect of the magnetic field on the flow of bihybrid and simple nanofluids piqued the interest of researchers as a controlling parameter. In many industrial processes, specifically product purification, slow fluid movement is obvious to complete the production successfully. Therefore, Figure 3a,b displays the

Table 3. Computations of the Local Thermal Gradient for the (Graphene–Ag)/Blood Bionanofluid at the Bottom and Top Ends of the Channel

| parameter changes | | | | | | | | local thermal gradient of BHNF versus the physical constraints | | | |
|-------------------|----------|-------|-----|-------|-------|------------|-------|--|------------------------|----------------------|------------------------|
| ϕ_{Ag} | ϕ_G | R_1 | M | R_d | Q_1 | θ_r | A_1 | $ \beta'(-1) $ | | $ \beta'(1) $ | |
| | 0.03 | 0.5 | 0.5 | 0.6 | 0.5 | 0.5 | 0.7 | expanding boundaries | contracting boundaries | expanding boundaries | contracting boundaries |
| 0.02 | | | | | | | | 0.4012 | 0.5692 | 0.1721 | 0.2879 |
| 0.04 | | | | | | | | 0.3904 | 0.4967 | 0.2384 | 0.3251 |
| 0.06 | | | | | | | | 0.3865 | 0.4639 | 0.2753 | 0.3431 |
| 0.08 | | | | | | | | 0.3848 | 0.4453 | 0.2985 | 0.3536 |
| 0.02 | 0.04 | | | | | | | 0.3947 | 0.5261 | 0.2095 | 0.3096 |
| | 0.08 | | | | | | | 0.3865 | 0.4563 | 0.2854 | 0.3473 |
| | 0.12 | | | | | | | 0.3847 | 0.4317 | 0.3175 | 0.3614 |
| | 0.16 | | | | | | | 0.3841 | 0.4193 | 0.3351 | 0.3688 |
| | 0.03 | 0.01 | | | | | | 0.1455 | 0.1999 | 0.4858 | 0.7829 |
| | | 0.03 | | | | | | 0.1496 | 0.2058 | 0.4771 | 0.7696 |
| | | 0.05 | | | | | | 0.1538 | 0.2118 | 0.4684 | 0.7565 |
| | | 0.07 | | | | | | 0.1580 | 0.2179 | 0.4598 | 0.7435 |
| | | 0.5 | 0.2 | | | | | 0.4136 | 0.5888 | 0.1645 | 0.2742 |
| | | | 0.4 | | | | | 0.4053 | 0.5758 | 0.1695 | 0.2833 |
| | | | 0.6 | | | | | 0.3971 | 0.5627 | 0.1746 | 0.2924 |
| | | | 0.8 | | | | | 0.3888 | 0.5497 | 0.1797 | 0.3016 |
| | | | 0.5 | 0.1 | | | | 0.4360 | 0.6132 | 0.1808 | 0.2605 |
| | | | | 0.3 | | | | 0.4223 | 0.5965 | 0.1781 | 0.2695 |
| | | | | 0.5 | | | | 0.4083 | 0.5787 | 0.1744 | 0.2809 |
| | | | | 0.7 | | | | 0.3940 | 0.5593 | 0.1693 | 0.2960 |
| | | | | 0.6 | 0.1 | | | 0.5042 | 0.7044 | 0.1455 | 0.2371 |
| | | | | | 0.2 | | | 0.4795 | 0.6725 | 0.1516 | 0.2486 |
| | | | | | 0.3 | | | 0.4541 | 0.6394 | 0.1581 | 0.2608 |
| | | | | | 0.4 | | | 0.4280 | 0.6050 | 0.1649 | 0.2739 |
| | | | | | 0.5 | 0.1 | | 0.4058 | 0.5628 | 0.1954 | 0.3215 |
| | | | | | | 0.2 | | 0.4031 | 0.5603 | 0.1906 | 0.3152 |
| | | | | | | 0.3 | | 0.4010 | 0.5597 | 0.1852 | 0.3077 |
| | | | | | | 0.4 | | 0.4001 | 0.5622 | 0.1791 | 0.2986 |
| | | | | | | 0.5 | 0.2 | 0.1769 | 0.2404 | 0.2857 | 0.4865 |
| | | | | | | | 0.4 | 0.2702 | 0.3783 | 0.2310 | 0.3917 |
| | | | | | | | 0.6 | 0.3593 | 0.5086 | 0.1887 | 0.3173 |
| | | | | | | | 0.8 | 0.4408 | 0.6259 | 0.1584 | 0.2637 |

control of the behavior of the fluids using a high Hartmann number. The results displayed in Figure 3a,b show that the fluid movement is very slow under a high Hartmann number in both hybrid and mono-nanoliquids as, physically, the value of M , the Lorentz force, which resists the fluid movement, becomes dominant. As a result, the maximum decrease in particle movement occurs. This optimum decrease is due to retarding effects of the applied magnetic force. The 3D view of Figure 3a,b is displayed in Figure 3c,d, respectively. Figure 3e,f depicts the velocity trends against the viscosity number R_1 in the case of expanding and contracting walls. The results revealed that a high viscosity number results in the most rapid decline in velocity and is dominant for hybrid nanoliquids. Physically, the viscous forces toward the successive layers of the fluid increase, which resist fluid movement. Further, the 3D analysis of Figure 3g,h is depicted in Figure 3i,j.

Figure 4 shows the temperature distribution in hybrid and mono-nanoliquids against the effects of increasing physical constraints. The temperature increase due to increasing values of the heat generation number Q_1 is illustrated in Figure 4a,b. The results highlight that the addition of heat-generating effects in the model is significant to acquire the maximum fluid temperature. The hybrid nanoliquid transmits heat more rapidly than the nanofluid. Physically, due to the cumulative thermal

conductivity of two types of nanoparticles, the resultant fluid becomes a good conductor; as a consequence, the heat transfer is rapid in contrast to that of a simple nanofluid. Further, expansion of the walls favors the temperature increase of both liquids and the thermal boundary layer elongates against the nanofluid. Figure 4c,d displays the 3D view of Figure 4a,b.

The investigation of the effects of quadratic radiations on the thermal distribution in nanofluids is a key research interest. Thus, the thermal enhancement in hybrid and simple nanoliquids under increasing thermal radiations (R_d) is illustrated in Figure 4e,f. It is found that the fluid achieved the maximum temperature variation when R_d changes from 0.1 to 0.4. Physically, quadratic radiations produce additional energy in the working fluid, and the fluid particles transmit this energy to the neighboring particles. Thus, the cumulative temperature of the fluid increases. Further, it is better to control the thermal boundary layer of the nanofluid, while it increases for the hybrid nanoliquid. Moreover, the 3D scenario of Figure 4e,f is displayed in Figure 4g,h. Figure 4i,j represents the temperature via the temperature ratio number θ_r , which appeared because of the quadratic radiation factor. The number θ_r boosts the heat transmission in hybrid and nanoliquids in an expanding/contracting channel. A fascinating 3D view of Figure 4i,j is provided in Figure 4k,l.

6. SHEAR DRAG AND LOCAL THERMAL GRADIENT (THE NUSSELT NUMBER)

This subsection highlights the computation of shear drag and local thermal gradient for the (graphene–Ag)/blood biohybrid nanofluid and includes the upper and lower ends of the working domain. Table 2 shows that the inclusion of more graphene in the blood causes the extension of shear drag at the lower side of the medium. On the other hand, the contraction of the walls may lead to an increase in the shear drag. Moreover, it is clear that by changing the concentration of nanoparticles while keeping other quantities unchanged, consequently, the shear drag uplifts at the upper plate of walls. It is obvious from the calculated results that the maximum shear drag is attained with a high viscosity number as compared to other physical parameters.

Table 3 helps investigate the thermal gradient behavior of nanofluids under the effects of various physical constraints. It is noticed that an improved thermal gradient can be achieved through the inclusion of more nanoparticles. However, elevated values were observed at the upper plate of the wall.

7. STUDY AND MODEL VALIDATION

The study and model validation via VIM is presented in this section. The results in Table 4 are computed considering $\phi_1 = \phi_2$

Table 4. Results of the Present Study and Model Validation with Previous Science Literature

| computation of the results for $F''(1)$ using VIM | | | |
|---|-------|----------------------------|---------------------------|
| M | A_1 | Bilal et al. ⁴⁹ | present results using VIM |
| 0 | 0.5 | 4.713254 | 4.713252 |
| 1 | | 4.739148 | 4.739139 |
| 2 | | 4.820361 | 4.820352 |
| 3 | | 4.396271 | 4.396268 |
| 2 | 0 | 1.842331 | 1.842330 |
| | 0.3 | 3.653601 | 3.653602 |
| | 0.6 | 5.391148 | 5.391143 |
| | 1 | 7.693006 | 7.693002 |

= 0 and $\alpha_1 = 0$, and it is obvious that these results are in excellent agreement with the results reported by Bilal et al.⁴⁹ This verifies the study and model validation via VIM.

8. CONCLUSIONS

This particular study is conducted on a biohybrid nanofluid model (BHNFM) under uniform expansion/contraction of walls. From the presented results, the following observations can be made:

- Because of the higher viscous forces caused by the composite density of Ag–G, the velocity of BHNFM is lower than that of MBNF (mono bionanofluid).
- The velocity inside the domain can be controlled for the desired purposes by strengthening the permeability and contraction of the boundaries.
- By placing a strong magnetic field on the channel, the movement of BHNFM and MBNF is greatly reduced, making it easier to control blood flow.
- By maximizing the heating species and quadratic radiations, the temperature of BHNFM and MBNF increases and is assessed as optimal for BHNFM.
- Both the expansion of the walls and the temperature quotient number θ_r increase the temperature of BHNFM and MBNF.

AUTHOR INFORMATION

Corresponding Author

Adnan – Department of Mathematics, Mohi-ud-Din Islamic University, Nerian Sharif 12080 AJ&K, Pakistan;
 orcid.org/0000-0003-0071-4743;
 Email: adnan_abbasi89@yahoo.com

Authors

Asla A. AL-Zahrani – Department of Chemistry, College of Science, Imam Abdulrahman Bin Faisal University, Dammam 31441, Saudi Arabia; Basic and Applied Scientific Research Center-College of Science-Imam Abdulrahman Bin Faisal Abdulrahman Bin Faisal University, Dammam 31441, Saudi Arabia

Ishtiaque Mahmood – Punjab University of Technology Rasul Mandi Bahauddin, Punjab 50370, Pakistan

Khaleeq ur Rahman – Department of Mathematics, Mohi-ud-Din Islamic University, Nerian Sharif 12080 AJ&K, Pakistan
Mutasem Z. Bani-Fwaz – Department of Chemistry, College of Science, King Khalid University, Abha 61413, Saudi Arabia;
 orcid.org/0000-0003-0426-1657

Elsayed Tag-Eldin – Center of Research, Faculty of Engineering, Future University in Egypt, New Cairo 11835, Egypt

Complete contact information is available at:

<https://pubs.acs.org/10.1021/acsomega.3c01903>

Notes

The authors declare no competing financial interest.

ACKNOWLEDGMENTS

The authors extend their appreciation to the Deanship of Scientific Research at King Khalid University for funding this work through large group Research Project under Grant Number RGP2/16/44.

NOMENCLATURE

| | |
|-----------------------------|--|
| \tilde{u}, \tilde{v} | velocity components (m/s) |
| \tilde{P} | pressure (Pa) |
| \tilde{T} | temperature (K) |
| $\mu_{\text{hbionanof}}$ | effective dynamic viscosity (kg/m·s) |
| $\rho_{\text{hbionanof}}$ | effective density (kg/m ³) |
| $k_{\text{hbionanof}}$ | effective thermal conductance (W/m·K) |
| $\sigma_{\text{hbionanof}}$ | enhanced electrical conductivity (S/m) |
| $(C_p)_{\text{hbionanof}}$ | enhanced heat capacity (J/K) |
| η | dimensionless variable |
| F' | dimensionless velocity |
| β | dimensionless temperature |
| R_d | thermal radiation number |
| θ_r | temperature ratio number |
| A_1 | permeability number |

REFERENCES

- (1) Mashayekhi, R.; Khodabandeh, E.; Akbari, O. A.; Toghraie, D.; Bahiraei, M.; Gholami, M. CFD analysis of thermal and hydrodynamic characteristics of hybrid nanofluid in a new designed sinusoidal double-layered microchannel heat sink. *J. Therm. Anal. Calorim.* **2018**, *134*, 2305–2315.
- (2) Bazdar, H.; Toghraie, D.; Pourfattah, F.; Akbari, O. A.; Nguyen, H. M.; Asadi, A. Numerical investigation of turbulent flow and heat transfer of nanofluid inside a wavy microchannel with different wavelengths. *J. Therm. Anal. Calorim.* **2020**, *139*, 2365–2380.
- (3) Arasteh, H.; Mashayekhi, R.; Goodarzi, M.; Motaharpour, S. H.; Dahari, M.; Toghraie, D. Heat and fluid flow analysis of metal foam

embedded in a double-layered sinusoidal heat sink under local thermal non-equilibrium condition using nanofluid. *J. Therm. Anal. Calorim.* **2019**, *138*, 1461–1476.

(4) He, W.; Ruhani, B.; Izadpanahi, N.; Esfahani, N. N.; Karimipour, A.; Afrand, M. Using of Artificial Neural Networks (ANNs) to predict the thermal conductivity of Zinc Oxide–Silver (50%–50%)/Water hybrid Newtonian nanofluid. *Int. Commun. Heat Mass Transfer* **2020**, *116*, No. 104645.

(5) Toghraie, D. A comprehensive experimental investigation of thermal conductivity of a ternary hybrid nanofluid containing MWCNTs- titania-zinc oxide/waterethylene glycol (80:20) as well as binary and mono nanofluids. *Synth. Met.* **2020**, *268*, No. 116501.

(6) Kristiawan, B.; Rifa'i, A. I.; Enoki, K.; Wijayanta, A. T.; Miyazaki, T. Enhancing the thermal performance of TiO₂/water nanofluids flowing in a helical microfin tube. *Powder Technol.* **2020**, *376*, 254–262.

(7) Kristiawan, B.; Wijayanta, A. T.; Enoki, K.; Miyazaki, T.; Aziz, M. Heat Transfer Enhancement of TiO₂/Water Nanofluids Flowing Inside a Square Minichannel with a Microfin Structure: A Numerical Investigation. *Energies* **2019**, *12*, No. 3041.

(8) Kurnia, J. C.; Chaedir, B.; Wijayanta, A. T.; Sasmito, A. P. Convective Heat Transfer Enhancement of Laminar Herschel–Bulkley Non-Newtonian Fluid in Straight and Helical Heat Exchangers with Twisted Tape Inserts. *Ind. Eng. Chem. Res.* **2022**, *61*, 814–844.

(9) Bhatti, M. M.; Bég, O. A.; Ellahi, R.; Doranehgard, M. H.; Rabiei, F. Electro-magnetohydrodynamics hybrid nanofluid flow with gold and magnesium oxide nanoparticles through vertical parallel plates. *J. Magn. Mater.* **2022**, *564*, No. 170136.

(10) Sait, S. M.; Sheremet, M. A.; Oztop, H. Thermal analysis and entropy generation of magnetic Eyring–Powell nanofluid with viscous dissipation in a wavy asymmetric channel. *Int. J. Numer. Methods Heat Fluid Flow* **2022**, 1609–1636.

(11) Muhammad, M. B.; Hakan, F. O.; Rahmat, E. Study of the Magnetized Hybrid Nanofluid Flow through a Flat Elastic Surface with Applications in Solar Energy. *Materials* **2022**, *15*, No. 7507.

(12) Zhang, L.; Tariq, N.; Mubashir, M. B. Study of nonlinear quadratic convection on magnetized viscous fluid flow over a non-Darcian circular elastic surface via spectral approach. *J. Taibah Univ. Sci.* **2023**, *17*, No. 2183702.

(13) Khan, Y.; Abdal, S.; Hussain, S.; Siddique, I. Numerical simulation for thermal enhancement of H₂O + Ethyl Glycol base hybrid nanofluid comprising GO+(Ag,AA7072,MoS₂). *AIMS Mathematics* **2023**, *8*, 11221–11237.

(14) Abbas, N.; Shatanawi, W.; Hasan, F.; Shatanawi, T. A. M. Numerical analysis of Darcy resistant Sutterby nanofluid flow with effect of radiation and chemical reaction over stretching cylinder: induced magnetic field. *AIMS Math.* **2023**, *8*, 11202–11220.

(15) Sadiq Murad, M. A.; Hamasalh, F. K.; Ismael, H. F. Numerical study of stagnation point flow of Casson-Carreau fluid over a continuous moving sheet. *AIMS Math.* **2023**, *8*, 7005–7020.

(16) Alsharari, F.; Mousa, M. M. New application of MOL-PACT for simulating buoyancy convection of a copper-water nanofluid in a square enclosure containing an insulated obstacle. *AIMS Math.* **2022**, *7*, 20292–20312.

(17) Ganesh, S.; Krishnambal, S. Magnetohydrodynamic Flow of Viscous Fluid Between Two Parallel Porous Plates. *J. Appl. Sci.* **2006**, *6*, 2420–2425.

(18) Ibrahim, W.; Shankar, B. MHD boundary layer flow and heat transfer of a nanofluid past a permeable stretching sheet with velocity, thermal and solutal slip boundary conditions. *Comput. Fluids* **2013**, *75*, 1–10.

(19) Srinivas, S.; Vijayalaxmi, A.; Ramamohan, T. R.; Reddy, A. S. Hydromagnetic Flow of a Nanofluid in a Porous Channel with Expanding or Contracting Walls. *J. Porous Media* **2014**, *17*, 953–967.

(20) Hafeez, H. Y.; Ndikilar, C. E. Flow of Viscous Fluid between Two Parallel Porous Plates with Bottom Injection and Top Suction. *Prog. Phys.* **2014**, *10*, 49–51.

(21) Fakour, M.; Vahabzadeh, A.; Ganji, D. D. Study of heat transfer and flow of nanofluid in permeable channel in the presence of magnetic field. *Propul. Power Res.* **2015**, *4*, 50–62.

(22) Mollamahdi, M.; Abbaszadeh, M.; Sheikhzadeh, G. A. Flow Field and Heat Transfer in a Channel with a Permeable Wall Filled with Al₂O₃-Cu/Water Micropolar Hybrid Nanofluid, Effects of Chemical Reaction and Magnetic Field. *J. Heat Mass Transfer Res.* **2016**, 101–114.

(23) Waqas, A.; Alghtani, A. H.; Anduaem, M. Thermal Transport in Radiative Nanofluids by Considering the Influence of Convective Heat Condition. *J. Nanomater.* **2022**, 1–11.

(24) Adnan, K.; Ilyas; Mohammad, A. Thermal transport investigation and shear drag at solid–liquid interface of modified permeable radiative-SRID subject to Darcy–Forchheimer fluid flow composed by γ -nanomaterial. *Sci. Rep.* **2022**, *12*, No. 3564.

(25) Mohyud-Din, S. T.; Khan, U.; Ahmed, N.; Abdeljawad, T.; Nisar, K. S. Thermal Transport Investigation in Magneto-Radiative GO-MoS₂/H₂O-C₂H₆O₂ Hybrid Nanofluid Subject to Cattaneo–Christov Model. *Molecules* **2020**, *25*, No. 2592.

(26) Vijayalakshmi, A.; Srinivas, S. Asymmetric Flow of a Nanofluid Between Expanding or Contracting Permeable Walls with Thermal Radiation. *Front. Heat Mass Transfer* **2016**, 11.

(27) Fakour, M.; Ganji, D. D.; Khalil, A.; Bakhshi, A. Heat Transfer in Nanofluids MHD Flow in Channel with Permeable Walls. *Heat Transfer Res.* **2017**, *48*, 221–238.

(28) Mehta, R.; Chouhan, V. S.; Mehta, T. Mhd flow of nanofluids in the presence of porous media, radiation and heat generation through a vertical channel. *J. Phys.: Conf. Ser.* **2019**, No. 012008.

(29) Chandrasekar, P.; Ganesh, S.; Ismail, A. M.; Anand, V. W. J. Magnetohydrodynamic flow of viscous fluid between two parallel porous plates with bottom injection and top suction subjected to an inclined magnetic field. *AIP Conf. Proc.* **2019**, No. 020144.

(30) Alhowaity, A.; Bilal, M.; Hamam, H.; Alqarni, M. M.; Mukdasai, K.; Aatif, A. Non-Fourier energy transmission in power-law hybrid nanofluid flow over a moving sheet. *Sci. Rep.* **2022**, *12*, No. 10406.

(31) Muhammad, B.; Ali, A.; Hejazi, H. A.; Mahmood, S. R. Numerical study of an electrically conducting hybrid nanofluid over a linearly extended sheet. *J. Appl. Math. Mech.* **2022**, No. e202200227.

(32) Alqahtani, A. M.; Bilal, M.; Usman, M.; Alsenani, T. R.; Samy, R. M.; Ali, A. Heat and mass transfer through MHD Darcy Forchheimer Casson hybrid nanofluid flow across an exponential stretching sheet. *J. Appl. Math. Mech.* **2023**, No. e202200213.

(33) Haq, I.; Bilal, M.; Ahammad, N. A.; Ghoneim, M. E.; Ali, A.; Weera, W. Mixed Convection Nanofluid Flow with Heat Source and Chemical Reaction over an Inclined Irregular Surface. *ACS Omega* **2022**, *7*, 30477–30485.

(34) Waini, I.; Ishak, A.; Pop, I. Hybrid nanofluid flow and heat transfer past a permeable stretching/shrinking surface with a convective boundary condition. *J. Phys.: Conf. Ser.* **2019**, No. 012022.

(35) Khan, K. A.; Raza, N.; Inc, M. Insights of numerical simulations of magnetohydrodynamic squeezing nanofluid flow through a channel with permeable walls. *Propul. Power Res.* **2021**, 412–420.

(36) Indumathi, N.; Ganga, B.; Jayaprakash, R.; Hakeem, A. K. A. Heat Transfer of Hybrid-nanofluids Flow Past a Permeable Flat Surface with Different Volume Fractions. *J. Appl. Comput. Mech.* **2022**, 21–35.

(37) Waqas, A. Numerical thermal featuring in γ Al₂O₃-C₂H₆O₂ nanofluid under the influence of thermal radiation and convective heat condition by inducing novel effects of effective Prandtl number model (EPNM). *Adv. Mech. Eng.* **2022**, 1–11.

(38) Murtaza, R.; Hussain, I.; Rehman, Z.; Khan, I.; Anduaem, M. Thermal enhancement in Falkner–Skan flow of the nanofluid by considering molecular diameter and freezing temperature. *Sci. Rep.* **2022**, *12*, No. 9415.

(39) Abbas, W.; Mutasem, Z. B.; Asogwa, K. K. Thermal efficiency of radiated tetra-hybrid nanofluid [(Al₂O₃-CuO-TiO₂-Ag)/water]tetra under permeability effects over vertically aligned cylinder subject to magnetic field and combined convection. *Sci. Prog.* **2023**, 1–17.

(40) Alharbi, K. A. M.; Adnan. Thermal investigation and physiochemical interaction of H₂O and C₂H₆O₂ saturated by Al₂O₃ and γ Al₂O₃ nanomaterials. *J. Appl. Biomater. Funct. Mater.* **2022**, No. 228080002211364.

- (41) Mburu, Z. M.; Mondal, S.; Sibanda, P. An Unsteady Nanofluid Flow Past Parallel Porous Plates: A Numerical Study. *Nanosci. Nanotechnol.* **2022**, *12*, 41–55.
- (42) Shaheen, A.; Imran, M.; Waqas, H.; Raza, M.; Rashid, S. Thermal transport analysis of squeezing hybrid nanofluid flow between two parallel plates. *Adv. Mech. Eng.* **2023**, *15*, 1–15.
- (43) Adnan. Heat Transfer Inspection in [(ZnO-MWCNTs)/Water-EG(50:50)]hnf with Thermal Radiation Ray and Convective Condition over a Riga Surface. In *Waves in Random and Complex Media*; Taylor & Francis, 2022; pp 1–15.
- (44) AlBaidani, M. M.; Mishra, N. K.; Alam, M. M.; Zahrani, A. A. A.; Akgul, A. Numerical Analysis of Magneto-Radiated Annular Fin Natural-Convective Heat Transfer Performance Using Advanced Ternary Nanofluid Considering Shape Factors with Heating Source. In *Case Studies in Thermal Engineering*; Elsevier, 2023; Vol. 44.
- (45) Khalid, A. K. A.; Ashraf, W.; Yassen, M. F.; Jamshed, W. Applied heat transfer modeling in conventional hybrid (Al₂O₃-CuO)/C₂H₆O₂ and modified-hybrid nanofluids (Al₂O₃-CuO-Fe₃O₄)/C₂H₆O₂ between slippery channel by using least square method (LSM). *AIMS Math.* **2023**, *8*, 4321–4341.
- (46) Adnan, K. M. A.; Abdulkhalik, M. Z. B.; Fwaz, F. Y.; Mansour Numerical Heat Performance of TiO₂/Glycerin under Nanoparticles Aggregation and Nonlinear Radiative Heat Flux in Dilating/Squeezing Channel. In *Case Studies in Thermal Engineering*; Elsevier, 2023; Vol. 41.
- (47) Pranowo; Wijayanta, A. T. Numerical Solution Strategy for Natural Convection Problems in a Triangular Cavity Using a Direct Meshless Local Petrov-Galerkin Method Combined with an Implicit Artificial-Compressibility Model. In *Engineering Analysis with Boundary Elements*; Elsevier, 2021; Vol. 126, pp 13–29.
- (48) Pranowo, D. A.; Makarim, A.; Suami, A. T.; Wijayanta, N.; Kobayashi; Itaya, Y. Marangoni convection within thermosolute and absorptive aqueous LiBr solution. *Int. J. Heat Mass Transfer* **2022**, *188*, No. 122621.
- (49) Bilal, M.; Arshad, H.; Ramzan, M.; Shah, Z.; Kumam, P. Unsteady hybrid-nanofluid flow comprising ferrous oxide and CNTs through porous horizontal channel with dilating/squeezing walls. *Sci. Rep.* **2021**, *11*, No. 12637.